1

Directive Ultra-Wideband Planar Antennas

A.-D. Capobianco #1, F.M. Pigozzo #2, A. Locatelli *3, D. Modotto *4, C. De Angelis *5, S. Boscolo +6, F. Sacchetto +7, M. Midrio +8
#*DEI, Università degli Studi di Padova*
**DEA, Università degli Studi di Brescia*
+*DIEGM, Università degli Studi di Udine*
Italy

1. Introduction

Since the acceptance of unlicensed use of the Ultra-Wideband (UWB) technology in the range between 3.1 and 10.6 GHz in the USA (FCC, 2002) and more recently between 3.4 and 8.5 GHz in Europe (ETSI, 2008), the realization of low-cost UWB wireless systems is considered a fundamental research goal both for military and commercial applications. The possible use and benefits of UWB technology are significant and among its potential applications, high-resolution radar and short-range ultra-high speed data transmission are very attractive. In this scenario, design, fabrication and characterization of effective antennas for UWB systems are challenging tasks with respect to the case of narrowband systems. A suitable UWB antenna should be capable of operating over an ultra-wide bandwidth. Therefore it is necessary to guarantee a good behavior of the antenna in the band of interest in terms of impedance matching with the transmitter, radiation and time-domain properties. Moreover, recent UWB antenna development tends to focus on ultra-compact planar antennas as they are more practical in terms of manufacturing, integration with the system electronics board and form factor. Typical configurations exhibit radiation patterns similar to the traditional monopole/dipole antennas, i.e. they behave as omnidirectional radiators in the plane normal to the radiating element. This feature is desirable in UWB devices which do not have a fixed or a-priori defined orientation with respect to the environment and thus when it is not necessary to favour any specific direction. On the other hand, strongly directive radiators are required for radar applications, especially when low-power, low-interference and high-resolution devices are needed. Directive UWB radiators are also interesting towards several complementary goals, e.g. to provide extra radio link gain to single antenna transceivers, to mitigate the effects of multipath in the indoor UWB channel, and, last but not least, to result in a high front-to-back ratio, which is desirable in many applications such as in wireless body-area networks (WBAN).
In the past few years, several printed broadband monopole-like configurations have been reported for UWB applications, but presently, very few efforts have been made to increase their directionality. This chapter intends to provide the reader with two different design methodologies for increasing the directivity of planar UWB antennas. In section 2, a novel antenna layout will be presented, as the result of subsequent modifications of a native

omnidirectional radiator: the bow-tie antenna. A high front-to-back ratio, low-profile design will be developed by exploiting a planar reflector and studying ad-hoc optimizations of both the antenna geometry and the feeding arrangement. The final layout could be particularly well-suited for point-to-point high data-rate UWB radio links around the 5.5 GHz center frequency.
In section 3, a different approach will be adopted: instead of backing an omnidirectional printed wideband dipole, a structured ground plane will be employed with a two-element array of disc monopoles. The resulting highly directive UWB antenna is designed to be used in combination with a single-chip radar transceiver operating between 6 and 8 GHz (Cacciatori et al., 2007).
The reader will find a detailed step-by-step design procedure, along with experimental data obtained through characterization of several prototypes in anechoic chamber.

2. An UWB Bow-Tie Antenna with High Front-to-Back Ratio

2.1 Design Principles

As previously said in the introduction of this chapter, in the UWB communication framework there are scenarios in which directivity is mandatory, for example when the antenna has to be located in the corner of a room or against a wall to provide a sectoral radio coverage from the transmitter (i.e. an access point) to the receiver (i.e. a set-top box). Moreover, small dimensions and low-profile are desirable features for an easier integration in the final device. For all these reasons the RF engineer may start the antenna design with the choice of the candidate wideband radiator along with its initial geometrical parameters. As directionality can be effectively achieved through the use of a planar reflector, the wide-band, planar radiating element can be natively omnidirectional, such as the bow-tie antenna. In the following, a design methodology is presented, starting from the technical specifications summarized in Table 1.

center frequency	5.5 GHz
fractional bandwidth	≥ 20%
laminate	Rogers RO4003C
laminate dimensions	30 x 50 mm^2
flat reflector dimensions	100 x 70 mm^2
laminate – reflector distance	roughly 5 mm

Table 1. Technical specifications.

The well known design guidelines for a bow-tie resonating at 5.5 GHz (Balanis, 2005) would lead to a total length of 16 mm, a small value that may cause problems when connecting the antenna to the feed-line whose dimensions are comparable with the radiator itself; this fact imposes to enlarge the antenna, and thus to force it to operate at a higher order resonance.
However, the laminate technical specifications limit the maximum size of the bow-tie. As a consequence, a good trade-off is the antenna layout shown in Fig. 1. The latter will in turn allow to save enough space to arrange the feeding/matching line on the same laminate. It is important to note that an antipodal configuration is preferable since the antenna will be fed using a 50 Ohm SMA connector.

Such an early model, mounted at a given distance above a planar reflector, can be studied and subsequently optimized through numerical simulations with CST Microwave Studio commercial software (CST, 2009).

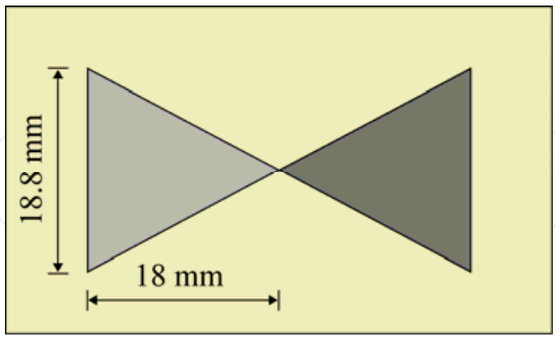

Fig. 1. The bow-tie planar wideband dipole. The reflector is omitted for sake of clarity. The dark (light) gray region is on the bottom (top) of the laminate, in antipodal configuration.

As shown in Fig. 2, the computed input impedance reveals a narrowband behavior, as the reactance is nearly zero over a small frequency range around the highest resonance; however, the real part is nearly constant between 6 and 8 GHz. This suggests to investigate a modified design to move down the highest resonance, as well as the flat resistance region, towards the 5.5 GHz center frequency.

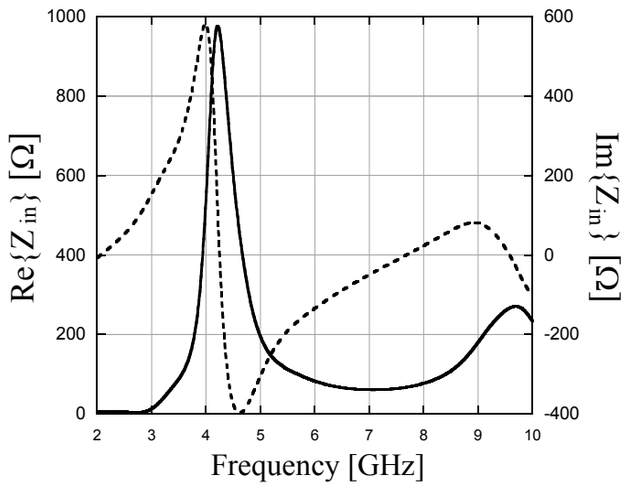

Fig. 2. Input impedance of the initial antenna of Fig. 1; real part (solid line) and imaginary part (dashed line).

Aiming to keep untouched the reference bow-tie dimensions, the effect of moving the feeding point off the vertex and along the edge of the patches can be numerically explored (see Fig. 3). In Figs. 4(a) and 4(b) the real and imaginary part of the input impedance are plotted versus frequency, for different values of the distance between the feeding point and the vertex. It is interesting to note that when this distance ("a"parameter in Fig. 3) ranges between 5 and 6 mm, the flat region of the real part of the input impedance falls in the band of interest, and the resonance approaches the desired center frequency of 5.5 GHz.

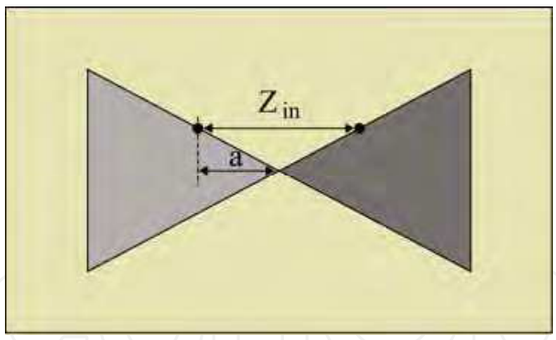

Fig. 3. Unconventional bow-tie feeding.

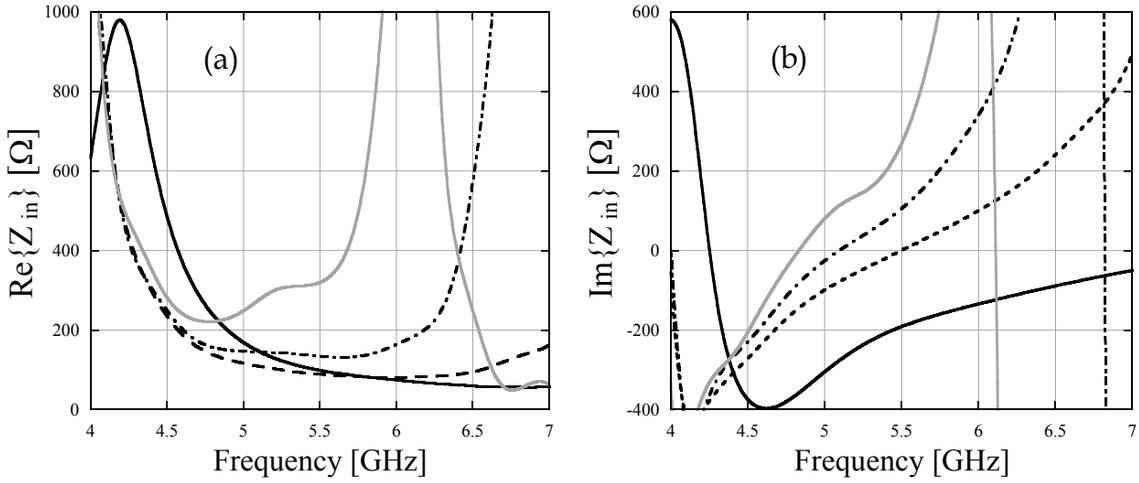

Fig. 4. (a) real part and (b) imaginary part of the input impedance versus frequency for different positions of the feeding point: a = 0 mm (solid line), a = 5 mm (dashed line), a = 6 mm (dashed-dotted line), a= 7 mm (gray line).

The next step in the design procedure is to provide a feasible microstrip transmission line to drive the signal up to the feeding points. A transmission line with 200 Ohm intrinsic impedance, a value which roughly coincides with the real part of the antenna input impedance, may be designed by suitably choosing the stripes widths and spacing (see Fig. 5(a)). Notice that, as in the case of many other planar transmission lines, the intrinsic impedance decreases for increasing strip widths. This in turn suggests that matching to a conventional 50 Ohm connector can be obtained by suitably tapering the strip widths.
Further refinements of the antenna resonance may be obtained by acting on the bow-tie tips, i.e. where the most intense currents flow. For instance, we observed that if we truncate the tip edges as shown in Fig. 5(b), a slight increase of the resonant frequency takes place (see Fig. 6, where the reflection coefficient of the antenna with and without the tips is reported).
If the antenna with truncated tips is chosen, two ways of designing the transmission line may be envisaged. Indeed, the stripes may be bent upward or downward from the feeding points. The latter option (see Fig. 7) is preferable, as a longer transmission line will in turn result in a smoother tapered transition to the 50 Ohm connector.

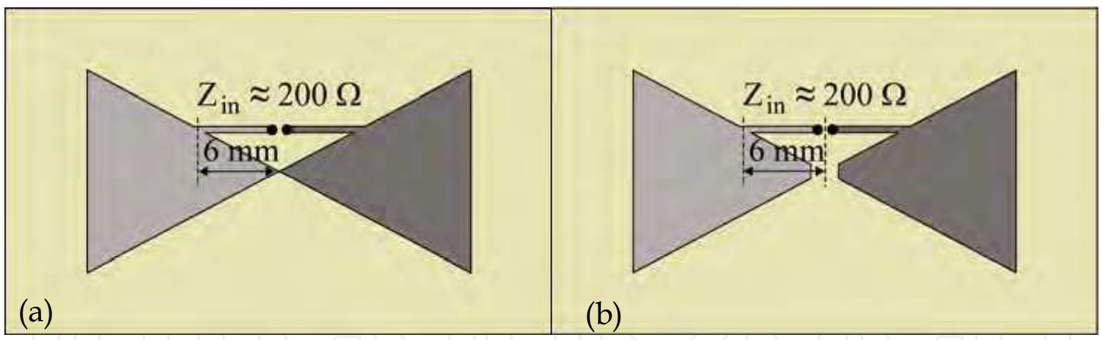

Fig. 5. Selected feeding point position and stripes arrangement: (a) with and (b) without bow-tie tips.

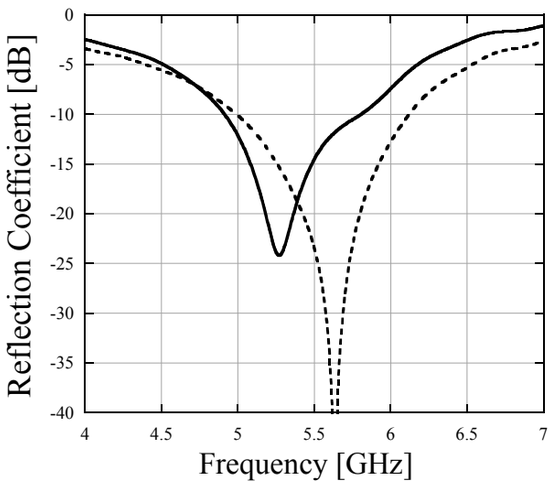

Fig. 6. Reflection coefficient of the antenna with off-vertex feeding: solid line refers to design of Fig. 5(a), dashed line refers to design of Fig. 5(b). In both cases, the reference impedance was set to 200 Ohm.

Bending the stripes downward will also cause the transmission line to run through the bow-tie truncated tips. As we will show in section 2.3, if the spacing between the line stripes and the truncated tips is small enough, two radiating *slots* (Balanis, 2005) are created. This will provide an additional resonance that may be tuned to further increase the overall antenna bandwidth.

2.2 Antenna Layout

Fig. 8 shows the final antenna layout. The laminate is a 50 x 30 x 1.575 mm^3 Rogers RO4003C mounted above a 110 x 90 mm^2 rectangular metal reflector (not depicted in the figure for sake of clarity) at a distance of 6 mm.
The thickness of the copper is 35 μm everywhere. A linear tapering of the feed-line ending with 3 mm width for the top layer and 8 mm width for the bottom layer provides the transition to the 50 Ohm SMA connector.

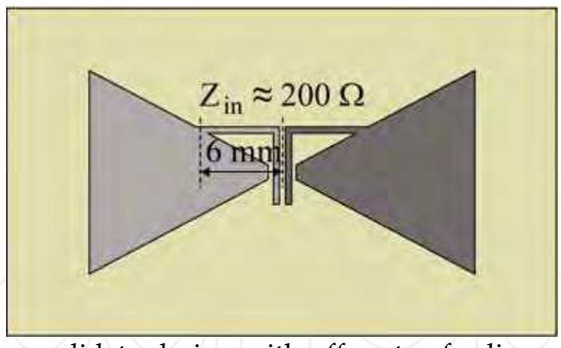

Fig. 7. Schematic of the candidate design with off-vertex feeding point, truncated bow-tie tips and bent feed-lines.

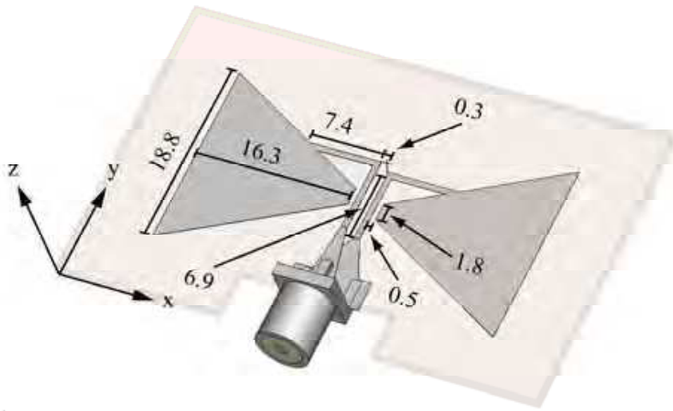

Fig. 8. Model and dimensions (in millimeters) of the proposed antenna. The left half of the planar radiator is on the top of the substrate, whereas the right half is on the bottom (antipodal configuration).

The parallel stripes which run between the bow-tie tips have a width equal to 0.6 mm. They are printed on opposite sides of the substrate and are separated by a 0.3 mm gap (with respect to the *x*-axis). The stripes are bent at a right angle and connect to the triangular patches via two 7.4 mm-long branches. The central vertex of each triangular patch is "cut away", resulting in a 0.5 x 1.8 mm² slot between the feed-line and the patch. The entire structure has been numerically modeled with CST Microwave Studio. All the elements have been included in the simulations: the metallic patches, stripes and planar reflector, as well as the SMA connector and the ending part of a 50 Ohm coaxial cable filled with lossy Teflon. All the metal parts have been regarded as perfect electric conductors, while the dielectrics in the laminate and in the coaxial cable have been modeled as lossy materials. Values $\varepsilon_r = 3.38$ and $\varepsilon_r = 2.1$ have been used for the relative permittivity of RO4003C and Teflon. As for the losses, $\tan\delta = 0.0027$ and $\tan\delta = 0.001$ have been used, respectively. Simulations have been performed in the 4 to 7 GHz range in order to optimize all the geometrical parameters of the antenna, including the dimensions of the stripes, the transition and the distance between the laminate and the reflector.

With the dimensions reported in Fig. 8, a prototype (Fig. 9) was fabricated using a numerically-controlled milling machine. Reflection coefficient and radiation patterns of the antenna under test have been measured in anechoic chamber using a 2-port Agilent N5230A

PNA-L network analyzer, a Satimo SGH-820 ridged horn wideband probe antenna, and a remotely controlled turntable.

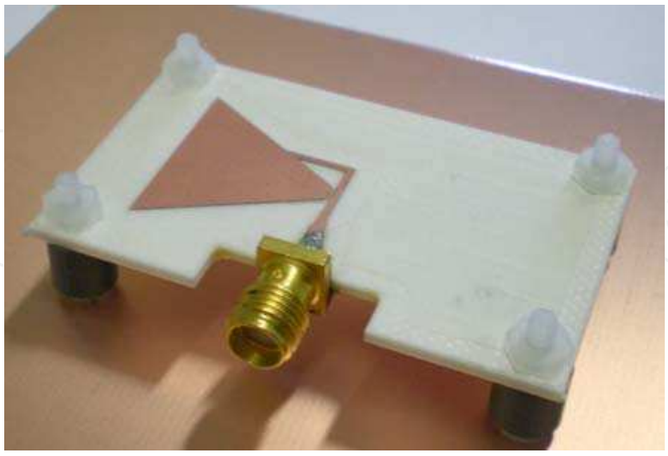

Fig. 9. Photograph of the antenna that has been fabricated and experimentally characterized.

2.3 The Radiation Mechanism

Figs. 10 and 11 show the simulated (dashed-dotted line) and measured (solid line) reflection coefficient (S_{11} parameter) and its representation on the Smith chart for the proposed antenna, as normalized to 50 Ohm. The measured band at $|S_{11}|$ = -10 dB spans from 4.8 GHz to 6.1 GHz. Therefore the bandwidth equals about a fourth of the center frequency, thus making the proposed bow-tie an Ultra-Wideband antenna, according to the FCC definition (FCC, 2002).

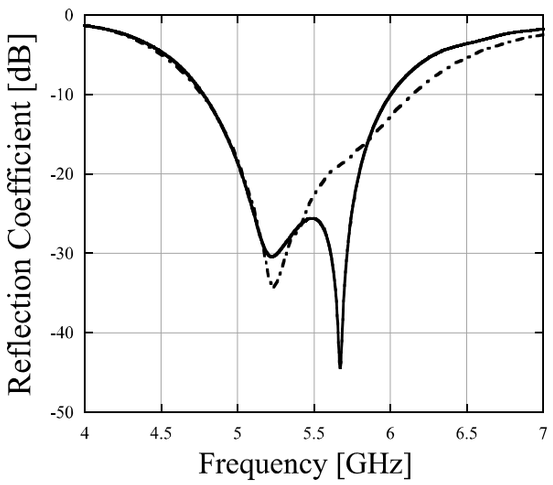

Fig. 10. Simulated (solid line) and measured (dashed-dotted line) magnitude of the reflection coefficient ($|S_{11}|$) versus frequency.

As for the radiation mechanism, we notice that the simulations clearly show two separate resonances which concur to form the antenna overall bandwidth. At the lower resonance, an

intense electric field is observed between the parallel stripes which run in the middle of the bow-tie tips. The stripes form a slot, loaded by the metallic patches which are connected at the slot far end by the T-branches. The resonant frequency scales inversely with the length of the parallel stripes.

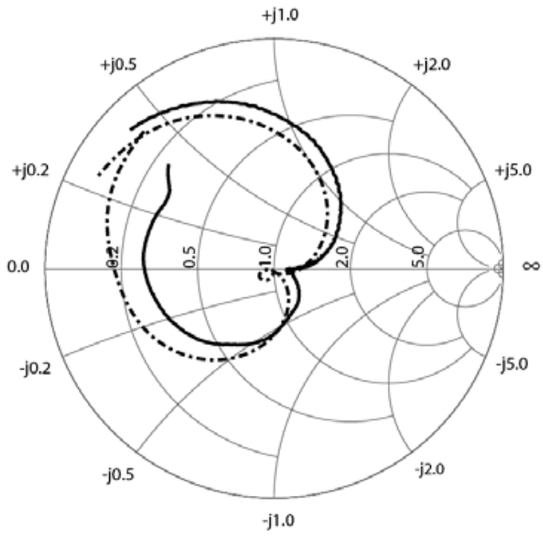

Fig. 11. Input impedance of the antenna on the Smith chart. Dashed-dotted line and solid line are used for simulated and measured data, respectively.

At the upper resonant frequency, radiation is due to the electric field which seeds in the slots etched between the parallel stripes and the bow-tie tips. The resonant frequency is influenced by the length of both the parallel stripes, and of the T-branches.

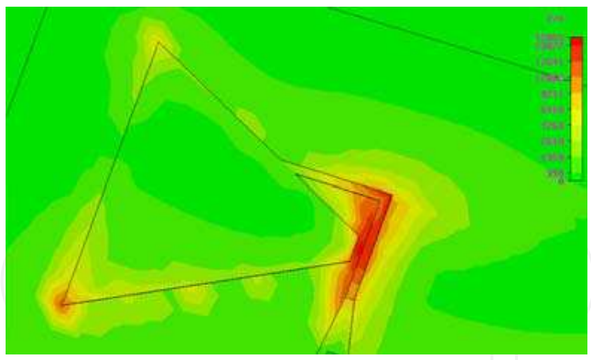

Fig. 12. Simulated surface magnetic currents intensity at the lower resonant frequency.

Figs. 12 and 13 confirm this picture by showing the numerically evaluated electric field at the two resonances. At the lower resonance (Fig. 12), a large electric field is observed all along the right-hand side of the feeding strip. Whereas, at the upper resonance (Fig. 13), it is clearly visible that the field no longer reaches the T-branch at the end of the strip. It is much more tightly confined in the region between the left-hand side of the strip and the truncated bow-tie tip, and rapidly vanishes away from the slot.

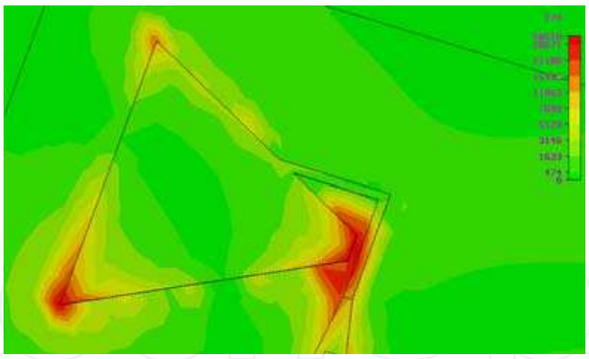

Fig. 13. Simulated surface magnetic currents intensity at the upper resonant frequency.

In the proposed antenna, therefore, the bow-tie is not used to realize a wideband radiator, as it is normally done in "conventional" bow-tie dipoles (Eldek et al., 2005), (Kiminami et al., 2004). Rather, the metallic patches are used as wideband loading or matching networks, and radiation is primarily due to magnetic currents which flow in properly designed slots.
Notice also that the two separate resonances we have observed in the simulations do not appear in the experimental results as clearly as in the simulations. We explain this discrepancy on the basis of the following considerations. When we numerically simulated the antenna, we observed that the spectral location of the upper resonant frequency is very sensitive to the electrical length of the T-branches. That is, small variations of either the physical length of these metallic stripes, or of the dielectric constant of the underlying slab may cause a noticeable shift of the upper resonant frequency. If the frequency shifts upwards, $|S_{11}|$ between the two resonances may eventually exceed the –10 dB level, finally splitting the operation bandwidth into two separate regions. Whereas, if the frequency shifts downward, the upper resonance tends to merge with the lower one, thus forming an unique dip in the $|S_{11}|$ plot. These behaviours are accompanied by easily detectable features on the Smith chart. Indeed, the two resonances form a loop near the chart center. The loop gets larger when the resonant frequencies split. Viceversa, it tends to collapse and to eventually disappear when the resonant frequencies merge. This is what happened in our experiment: the loop in the vicinity of the chart center has a very reduced extension, revealing that the two resonant frequencies have merged. The likely cause is either a misfabrication, or a slight discrepancy between the experimental and declared values of the dielectric constant.

2.4 Radiation Patterns, Front-to-Back Ratio, and Group Delay

Figs. 14, 15 and 16 show the radiation patterns in the *x-z* and *y-z* planes for the 4.8 GHz, 5.5 GHz and 6.1 GHz frequencies respectively. The -3 dB beamwidth ranges between 52 and 87 degrees and between 60 and 72 degrees in the *x-z* and *y-z* planes respectively. It may be observed that the direction of maximum radiation is slightly off the normal to the plane which contains the antenna. This is due to the antipodal layout of the antenna itself.
Fig. 17 shows the measured frequency dependence of the front-to-back ratio, which always exceeds the level of 24 dB. The measured antenna gain ranges between 8 and 10 dB.
As for the antenna performance in the time-domain, we calculated the variation in frequency of the group delay, which is related to the first-derivative of the measured phase of the S_{12} parameter. As can be seen in Fig. 18 the variation of the group delay in the band of

interest is less than 250 ps, which is appreciably low as compared to the duration of the stimulus in a pulsed transmission (about 1.5 ns for the 4.8 - 6.1 GHz band).

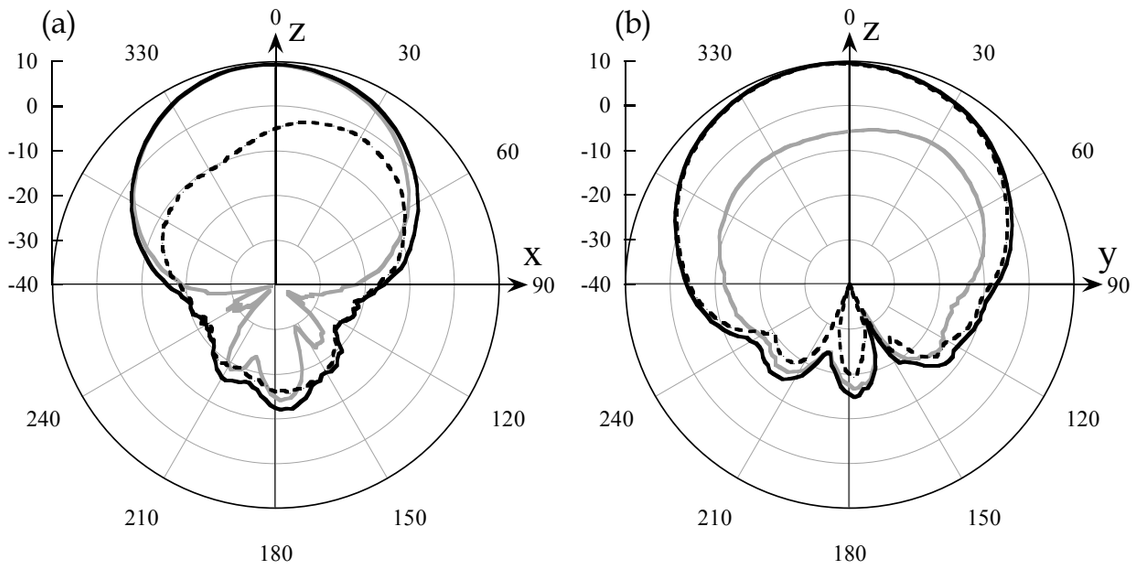

Fig. 14. Measured radiation patterns at 4.8 GHz; (a) in the *x*-*z* plane, (b) in the *y*-*z* plane. Gray line: in-plane electric field; dashed-line: electric field orthogonal to the plane; solid-line: total electric field. The results are reported in dB.

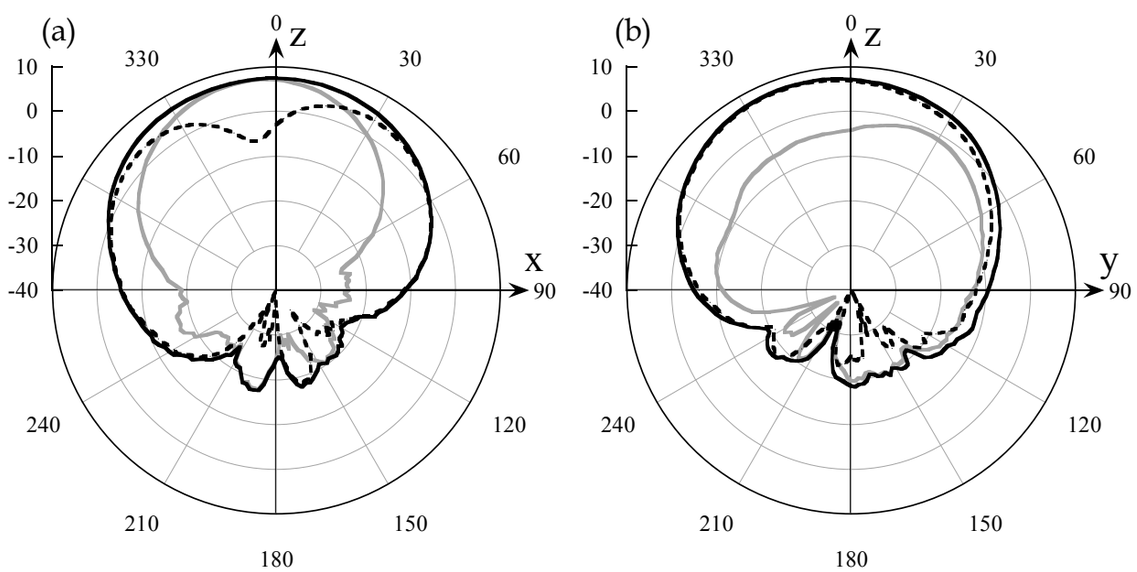

Fig. 15. Measured radiation patterns at 5.5 GHz; (a) in the *x*-*z* plane, (b) in the *y*-*z* plane. Gray line: in-plane electric field; dashed-line: electric field orthogonal to the plane; solid-line: total electric field. The results are reported in dB.

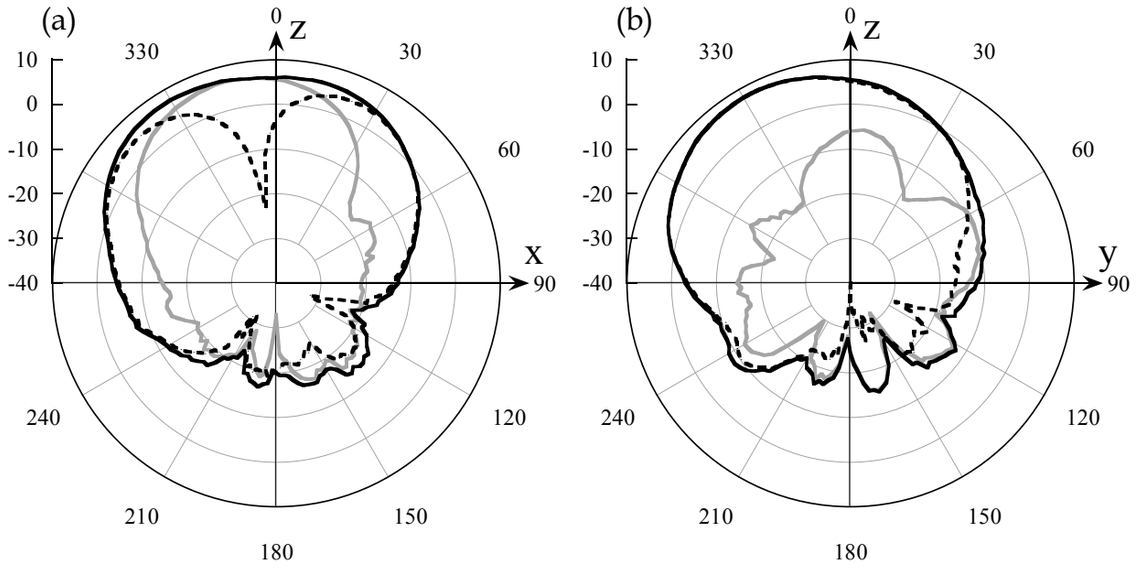

Fig. 16. Measured radiation patterns at 6.1 GHz; (a) in the *x-z* plane, (b) in the *y-z* plane. Gray line: in-plane electric field; dashed-line: electric field orthogonal to the plane; solid-line: total electric field. The results are reported in dB.

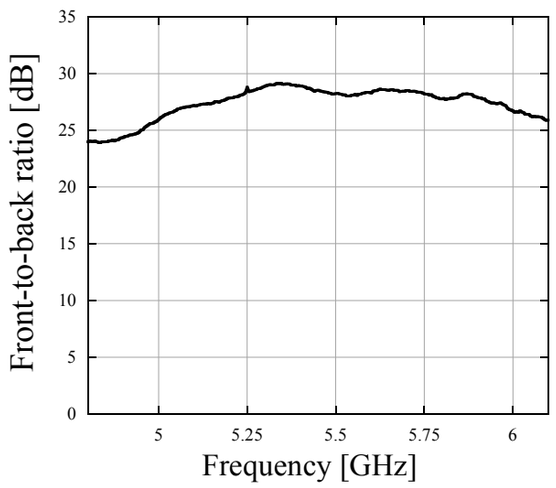

Fig. 17. Measured front-to-back ratio in the frequency range 4.8 – 6.1 GHz.

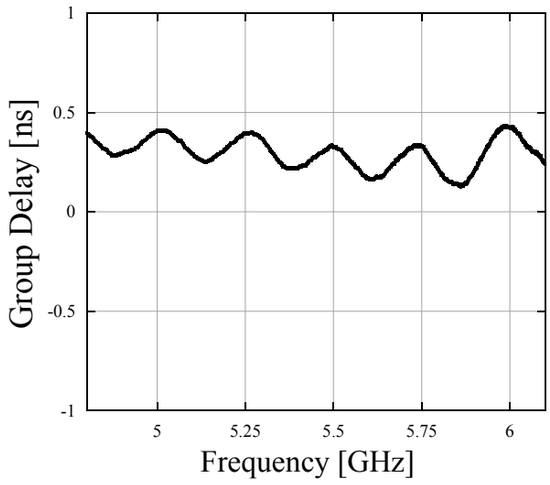

Fig. 18. Measured group delay in the frequency range 4.8 – 6.1 GHz.

3. A Planar, Differential, and Directive Ultra-Wideband Antenna

In this section a planar differential UWB antenna characterized by high directivity is described. The proposed structure is composed of two disc monopoles with L-shaped ground planes, fed by 50 Ohm microstrip lines (100 Ohm differential input). The introduction of a structured ground plane and the array effect permit to achieve a measured gain exceeding 11 dB even on a low-cost substrate, maintaining at the same time a reasonable size of the board. As reference application, the antenna has been optimized to work between 6 and 8 GHz in combination with a single-chip radar transceiver (Cacciatori et al., 2007).

3.1 Antenna Layout

A sketch of the differential UWB antenna is reported in Fig. 19. The structure is formed by two disc monopoles with L-shaped ground planes, fed by 50 Ohm microstrip lines (width equal to 3 mm), on a low-cost FR4 substrate. We assumed that the FR4 dielectric constant is 4.5, and the declared board thickness is equal to 1.6 mm. Optimization of the antenna was performed through CST Microwave Studio simulations, and the reported results correspond to the device with the geometric parameters that guarantee the best theoretical performance. In Fig. 19 we show the size of the board, and the position of the centers of the two disc monopoles, whose radius is 9 mm.

The basic element of the proposed differential antenna is the single disc monopole, with the related 50 Ohm microstrip feed-line and the L-shaped ground plane with rounded corner. The distance between the edge of each disc and the horizontal and vertical metal stripes that compose the L-shaped ground plane is 1 and 2 mm respectively. This building block (50 x 50 mm^2) is then rotated by 40 degrees in the *x-y* plane, and it is depicted within a yellow square in Fig. 19. The second element of the array is obtained by mirroring the first one with respect to the x = 0 plane. The region between the two elements on the ground side is filled with metal, so that this large common ground plane can be exploited for a straightforward placement of a single-chip transceiver and its circuitry. As shown in Fig. 19, the distance

between the two disc monopoles is about 70 mm, which is larger than the maximum signal wavelength. In Fig. 20 a photograph of the fabricated antenna is reported.

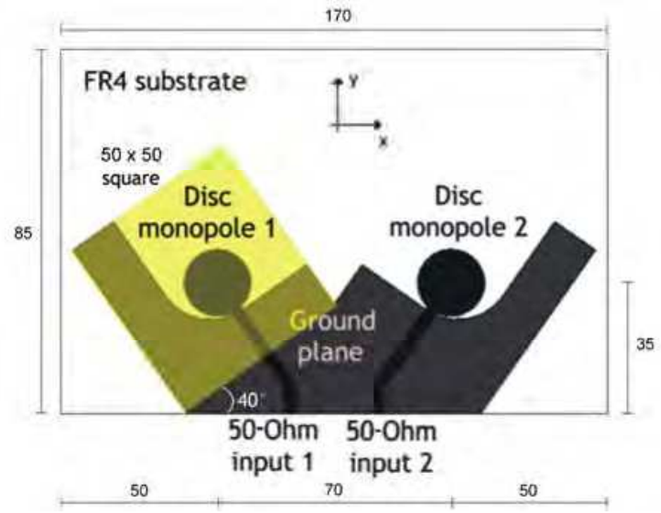

Fig. 19. Sketch of the differential UWB antenna: disc monopoles and microstrip lines (black), structured ground plane (dark gray) and the basic element of the array (yellow square) are depicted. The dimensions are in millimeters.

3.2 Reflection Coefficient, Group Delay and Radiation Patterns

Differential and common-mode reflection coefficients ($|S_{dd}|$ and $|S_{cc}|$) have been measured by using a 4-port vector network analyzer Anritsu MS4624D, whereas the single-port reflection coefficient at port 1 ($|S_{11}|$) has been measured through a 2-port Agilent N5230A PNA-L network analyzer. In Fig. 21 we report results obtained from measurements between 4 and 9 GHz; it is worth noting that the three curves are almost overlapped and this implies that, as desired, coupling between the two antenna elements is very weak. The differential reflection coefficient is below -10 dB in the frequency range between 5.3 and 9 GHz, thus the differential UWB antenna exhibits a good behavior in terms of impedance matching over a bandwidth larger than 4 GHz. Also the group delay has been measured in anechoic chamber, by using the same setup we have used for measurements of gain and radiation patterns (see below for the setup description). The results are reported in Fig. 22: it is fundamental to note that the maximum group delay variation is equal to fractions of a nanosecond, therefore the antenna is able to guarantee low pulse distortion.

The radiative properties of the differential UWB antenna have been characterized in anechoic chamber by utilizing a 2-port Agilent N5230A PNA-L network analyzer, two 180-degree hybrid couplers, a Satimo SGH-820 ridged horn wideband probe antenna, and a remotely controlled turntable. Here we report the results for co-polarization at 7 GHz; we emphasize the fact that the level of cross-polarization is quite low, and the shape of the radiation patterns is rather uniform over the entire band.

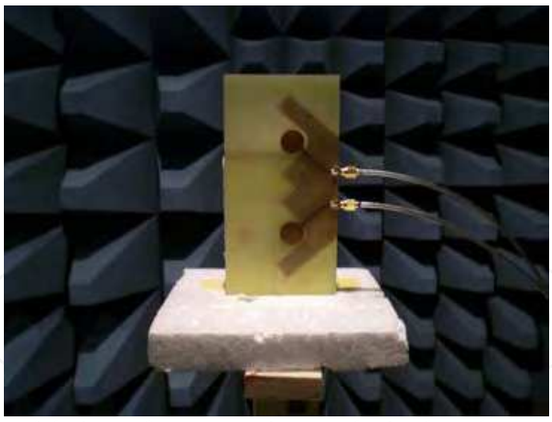

Fig. 20. Photograph of the fabricated antenna in anechoic chamber.

In Fig. 23(a) we show measured and simulated radiation pattern in the *x*-*y* plane when only port 1 is excited. The results show the typical behavior of a disc monopole with L-shaped ground plane, with a single lobe of radiation oriented along the *y*-axis, and the maximum gain is equal to 8.6 dB. In Figs. 23(b) and 24(a) we report measured and simulated radiation patterns in the *x*-*y* and *y*-*z* plane respectively, when the two input ports are excited with signals with opposite polarity. The increase of directionality is clearly visible even from a simple analysis of the shape of the patterns: indeed, the maximum gain is equal to 11.6 dB. In Fig. 24(b) we report, for the sake of comparison, measured and simulated radiation patterns for in-phase excitation of the two ports in the *x*-*y* plane. It is possible to note the birth of two lobes, with a maximum gain equal to 9.1 dB. In all the cases, it is worth noting the excellent agreement between numerical and experimental data. These results clearly demonstrate that the proposed differential UWB antenna is a good candidate to be used whenever a highly directive differential radiator with planar profile is required.

3.3 The Radiation Mechanism

We have numerically investigated the pattern of the surface currents on the UWB differential antenna, in order to identify the reasons for such a huge increase of directionality. The usage of a disc monopole with L-shaped ground plane guarantees the suppression of one lobe of radiation with respect to conventional monopoles, and this corresponds to an increase of gain of about 3 dB. The two disc monopoles that compose the differential antenna can be considered as an array of two elements, wherein each element radiates with only one main lobe of radiation along the *y*-direction. The structure should ideally behave as a broad-side array, with maximum value of the array factor in normal direction with respect to the alignment direction (i.e. *x*-axis) (Someda, 1998). From the theory of antenna arrays, it is well known that we get a broad-side array when the current distribution on each antenna element is in phase.

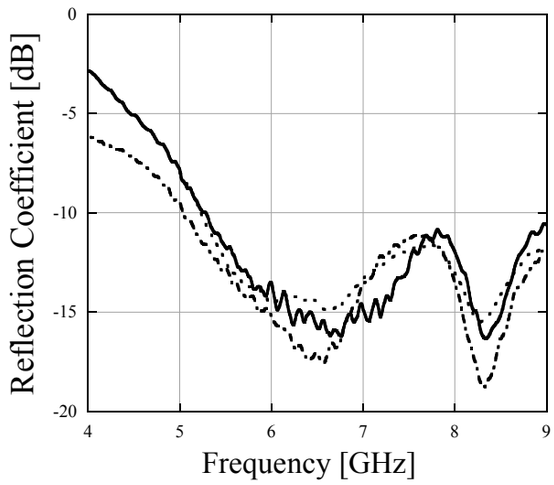

Fig. 21. Measured differential (solid line) and common-mode (dashed-dotted line) reflection coefficients $|S_{dd}|$ and $|S_{cc}|$, and measured single-port reflection coefficient $|S_{11}|$ (dotted line) between 4 and 9 GHz.

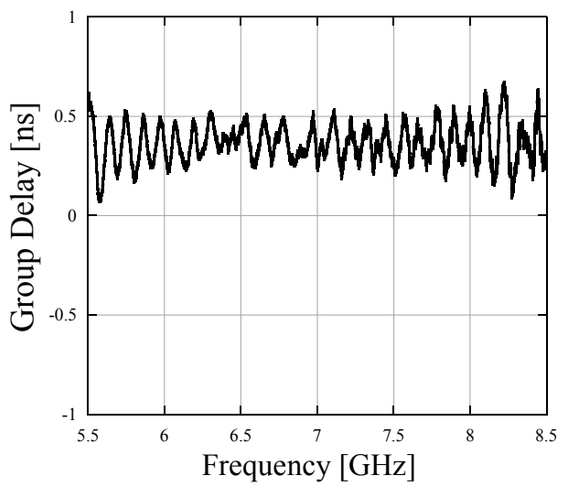

Fig. 22. Measured group delay curve between 5.5 and 8.5 GHz.

In Fig. 25 we plot the *y*-component of the surface currents at 7 GHz for differential input (the two ports have opposite polarity). It is straightforward to see that the currents on the microstrips have opposite polarity, whereas on the radiating elements they are predominantly distributed on the edge of the discs and are in phase due to the mirror symmetry between the two elements. As a consequence, in this case the differential antenna behaves as a broad-side array, as shown by the radiation pattern in Fig. 23(b). Viceversa, when the two input ports are fed in phase the currents on the two microstrips are obviously in phase, whereas on the radiating elements they are out of phase. Indeed, the radiation pattern in Fig. 24(b) exhibits two radiation lobes and no enhancement of directivity, as predicted by the calculation of the array factor. Notice that the increase of gain in the case of differential input with respect to excitation of a single port is about 3 dB, which is exactly the value predicted by the theory of antenna arrays for a two-element array.

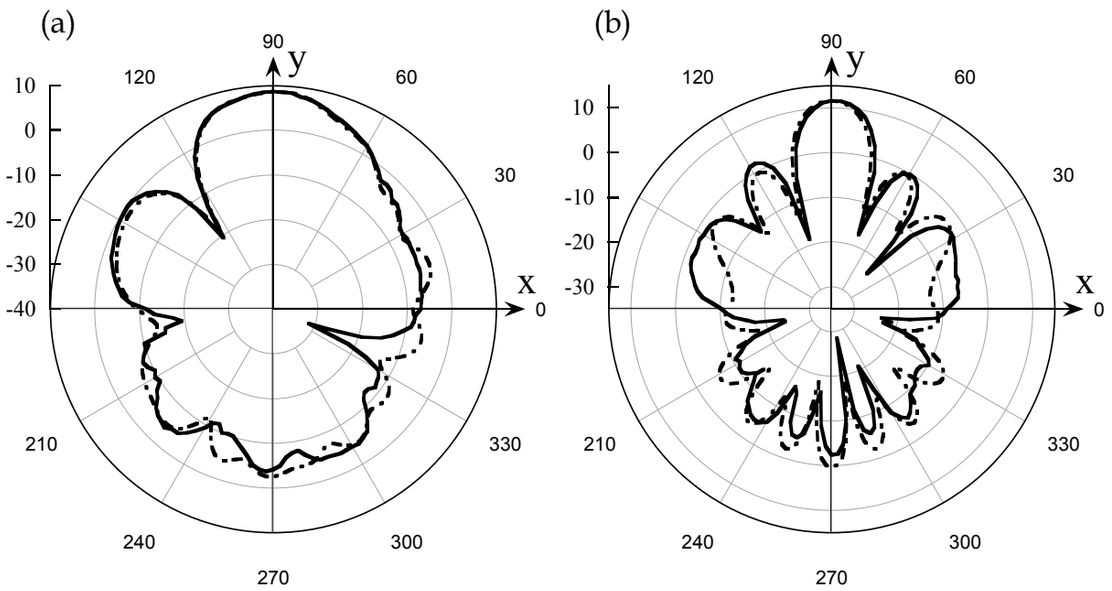

Fig. 23. Measured (solid line) and simulated (dashed-dotted line) radiation patterns in the *x-y* plane for in-plane polarization at 7 GHz. (a) Only port 1 was excited, maximum gain is 8.6 dB. (b) port 1 and port 2 are excited with opposite polarity (differential excitation), maximum gain is 11.6 dB. The results are reported in dB.

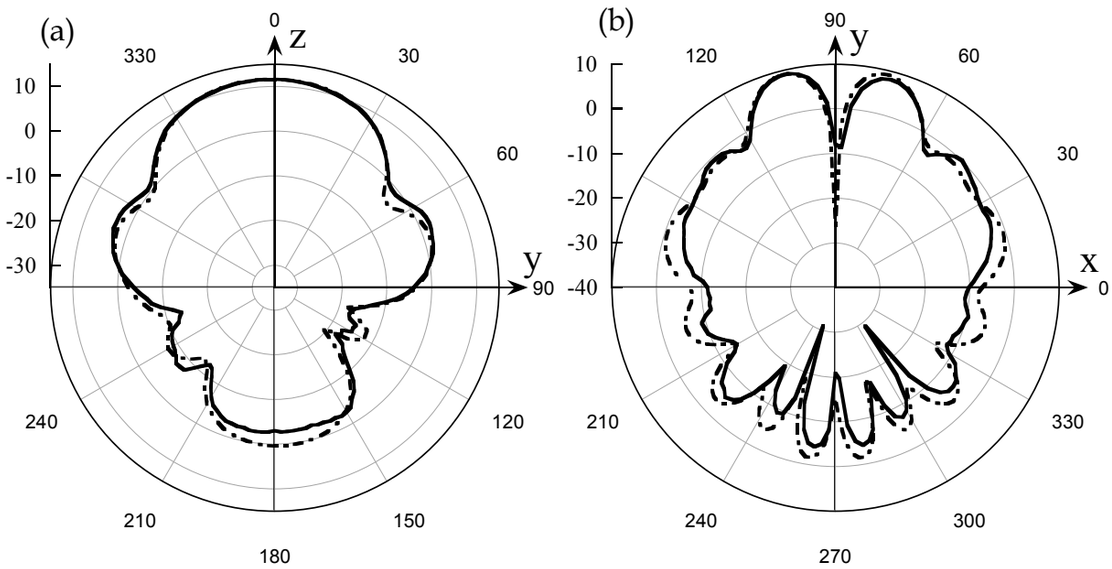

Fig. 24. Measured (solid line) and simulated (dashed-dotted line) radiation patterns for in-plane polarization at 7 GHz. (a) *y-z* plane, differential excitation. (b) *x-y* plane, port 1 and port 2 are excited with the same polarity, maximum gain is 9 dB. The results are reported in dB.

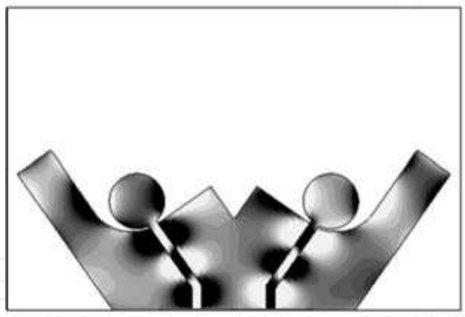

Fig. 25. Plot of the *y*-component of the surface currents at 7 GHz, white (black) represents positive (negative) values. The two ports are excited with opposite polarity.

3.4 Gain

In Fig. 26 we report measured and simulated gain in the band of interest for the case of differential excitation. The two curves exhibit good agreement, in spite of the high degree of uncertainty associated with the electromagnetic parameters of the FR4 substrate. In particular, in all the simulations we took a dielectric loss tangent tan $\delta = 0.02$, which seems to be a reasonable value according to what is commonly reported in the literature. It is worth noting that the gain curves are quite flat, with values between 10 and 12 dB over the entire bandwidth. In the same figure we also report simulations that show the gain that could be achieved by fabricating the same structure on a more expensive substrate designed for RF, and thus characterized by negligible loss tangent. We have found that the maximum gain would be between 11.5 and 13.5 dB: it is worth noting that these are huge values for a structure with planar profile.

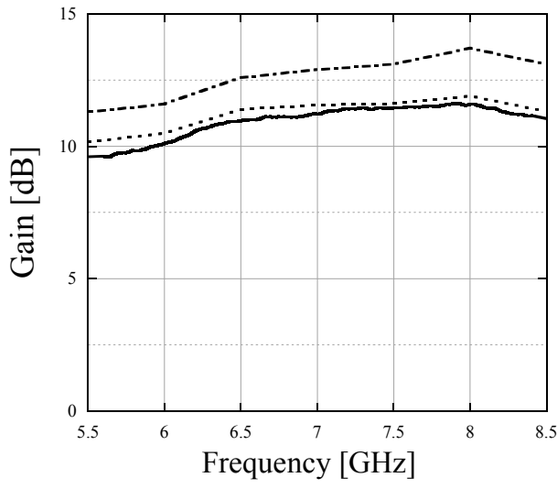

Fig. 26. Measured (solid line) and simulated (dotted line) gain of the fabricated antenna with differential excitation, and simulated gain of the same structure by considering negligible losses in the dielectric substrate (dashed-dotted line).

4. Conclusion

The logical thread of this chapter can be summarized as follows. Highly directive, planar UWB antennas are gaining more and more attention, as required in many novel and important applications. As the modern antenna design deals with low profile structures, new ways of increasing the directivity of a candidate radiator can be explored. Two different techniques were presented throughout this chapter. In Section 2, the operation of a novel bow-tie antenna with high front-to-back ratio and directivity has been demonstrated. This unconventional bow-tie antenna exploits magnetic currents excited in properly designed slots, while the two metallic patches act as a wideband loading or matching network. A prototype has been fabricated and characterized using a vector network analyzer in an anechoic chamber demonstrating the effectiveness of the proposed design in the 4.8 - 6.1 GHz band. In Section 3 we have presented a differential planar UWB antenna characterized by higher gain (more than 11 dB around 7 GHz) with respect to conventional printed radiators. The presence of a large common ground plane is a key feature in order to simplify placement of single-chip UWB transceivers, which typically have a differential input/output structure: as a consequence, direct connection between chip and antenna would be possible, without resorting to baluns. The antenna has been fabricated on a low-cost FR4 substrate and has been completely characterized: both simulations and measurements performed in anechoic chamber have demonstrated that the strong increase of directionality is mainly due to the presence of a carefully structured ground plane and to the array effect.

5. References

Balanis, C. A. (2005). *Antenna theory, analysis and design,* John Wiley & Sons, ISBN: 0-471-66-782-X, Hoboken, New Jersey.

Cacciatori, A.; Lorenzi, L. & Colalongo, L. (2007). A Power Efficient HBT Pulse Generator for UWB Radars. *Proceedings of ISCAS 2007*, pp. 3916-3919, ISBN: 1-4244-0920-9, New Orleans, May 2007.

CST Microwave Studio (2009), Darmstadt, Germany.

Eldek, A. A.; Elsherbeni, A. Z. & Smith, C. E. (2005). Wide-Band Modified Printed Bow-Tie Antenna With Single and Dual Polarization for C– and X-Band Applications. *IEEE Transactions on Antennas and Propagation,* Vol. 53, September 2005, pp. 3067-3072, ISSN: 0018-926X.

European Telecommunications Standards Institute (ETSI), *Ultra Wideband (UWB) technologies for communication purposes,* ETSI EN 302 065 V1.1.1 (2008-02), February 2008.

Federal Communications Commission (FCC), *Revision of Part 15 of the Commission's Rules Regarding Ultra-Wideband Transmission Systems,* First Report and Order, FCC 02-48, 2002.

Kiminami, K.; Hirata, A. & Shiozawa, T. (2004). Double-Sided Printed Bow-Tie Antenna for UWB Communications. *IEEE Antennas and Wireless Propagation Letters,* Vol. 3, 2004, pp. 152-153, ISSN: 1536-1225.

Someda, C. G. (1998). *Electromagnetic Waves*, Chapman & Hall, ISBN: 0-412-57870-0, London, UK.

Microwave and Millimeter Wave Technologies Modern UWB antennas and equipment

Edited by Igor Mini

ISBN 978-953-7619-67-1
Hard cover, 488 pages
Publisher InTech
Published online 01, March, 2010
Published in print edition March, 2010

How to reference

In order to correctly reference this scholarly work, feel free to copy and paste the following:

A.-D. Capobianco, F.M. Pigozzo, A. Locatelli, D. Modotto, C. De Angelis, S. Boscolo, F. Sacchetto, M. Midrio (2010). Directive Ultra-Wideband Planar Antennas, Microwave and Millimeter Wave Technologies Modern UWB antennas and equipment, Igor Mini (Ed.), ISBN: 978-953-7619-67-1, InTech, Available from: http://www.intechopen.com/books/microwave-and-millimeter-wave-technologies-modern-uwb-antennas-and-equipment/directive-ultra-wideband-planar-antennas

INTECH
open science | open minds

InTech Europe
University Campus STeP Ri
Slavka Krautzeka 83/A
51000 Rijeka, Croatia
Phone: +385 (51) 770 447
Fax: +385 (51) 686 166
www.intechopen.com

InTech China
Unit 405, Office Block, Hotel Equatorial Shanghai
No.65, Yan An Road (West), Shanghai, 200040, China
中国上海市延安西路65号上海国际贵都大饭店办公楼405单元
Phone: +86-21-62489820
Fax: +86-21-62489821

IntechOpen